Characterizing brown dwarf companions with IRDIS long-slit spectroscopy: HD 1160 B and HD 19467 B

D. Mesa, V. D'orazi, Arthur Vigan, D Kitzmann, K Heng, R. Gratton, S. Desidera, M. Bonnefoy, B. Lavie, A-L Maire, et al.

▶ **To cite this version:**

D. Mesa, V. D'orazi, Arthur Vigan, D Kitzmann, K Heng, et al.. Characterizing brown dwarf companions with IRDIS long-slit spectroscopy: HD 1160 B and HD 19467 B. Monthly Notices of the Royal Astronomical Society, 2020, 495 (4), pp.4279-4290. 10.1093/mnras/staa1444 . hal-02898999

HAL Id: hal-02898999
https://hal.science/hal-02898999v1

Submitted on 1 Sep 2023

HAL is a multi-disciplinary open access archive for the deposit and dissemination of scientific research documents, whether they are published or not. The documents may come from teaching and research institutions in France or abroad, or from public or private research centers.

L'archive ouverte pluridisciplinaire **HAL**, est destinée au dépôt et à la diffusion de documents scientifiques de niveau recherche, publiés ou non, émanant des établissements d'enseignement et de recherche français ou étrangers, des laboratoires publics ou privés.

Monthly Notices
of the
ROYAL ASTRONOMICAL SOCIETY

MNRAS **495,** 4279–4290 (2020)
Advance Access publication 2020 May 23

doi:10.1093/mnras/staa1444

Characterizing brown dwarf companions with IRDIS long-slit spectroscopy: HD 1160 B and HD 19467 B

D. Mesa,[1]★ V. D'Orazi,[1,2] A. Vigan,[3] D. Kitzmann,[4] K. Heng,[4,5] R. Gratton,[1] S. Desidera,[1] M. Bonnefoy,[6] B. Lavie,[7] A.-L. Maire,[8] S. Peretti[7] and A. Boccaletti[9]

[1]*INAF-Osservatorio Astronomico di Padova, Vicolo dell'Osservatorio 5, I-35122 Padova, Italy*
[2]*School of Physics and Astronomy, Monash University, Clayton Campus, Victoria 3800, Melbourne, Australia*
[3]*Aix Marseille Université, CNRS, LAM, UMR 7326, F-13388, Marseille, France*
[4]*Center for Space and Habitability, University of Bern, Gesellschaftsstrasse 6, CH-3012 Bern, Switzerland*
[5]*Department of Physics, Astronomy & Astrophysics Group, University of Warwick, Coventry CV4 7AL, UK*
[6]*Univ. Grenoble Alpes, CNRS, IPAG, F-38000 Grenoble, France*
[7]*Geneva Observatory, University of Geneva, Chemin des Maillettes 51, CH-1290 Versoix, Switzerland*
[8]*STAR Institute, Université de Liège, Allée du Six Août 19c, B-4000 Liège, Belgium*
[9]*LESIA, Observatoire de Paris, Université PSL, CNRS, Sorbonne Université, Univ. Paris Diderot, Sorbonne Paris Cité, 5 place Jules Janssen, F-92195 Meudon, France*

Accepted 2020 May 19. Received 2020 May 19; in original form 2020 April 9

ABSTRACT

The determination of the fundamental properties (mass, separation, age, gravity, and atmospheric properties) of brown dwarf companions allows us to infer crucial informations on their formation and evolution mechanisms. Spectroscopy of substellar companions is available to date only for a limited number of objects (and mostly at very low resolution, $R < 50$) because of technical limitations, i.e. contrast and angular resolution. We present medium resolution ($R = 350$), coronagraphic long-slit spectroscopic observations with SPHERE of two substellar companions, HD 1160 B and HD 19467 B. We found that HD 1160 B has a peculiar spectrum that cannot be fitted by spectra in current spectral libraries. A good fit is possible only considering separately the Y+J and the H spectral band. The spectral type is between M5 and M7. We also estimated a $T_{\rm eff}$ of 2800–2900 K and a $\log g$ of 3.5–4.0 dex. The low surface gravity seems to favour young age (10–20 Myr) and low mass ($\sim$20 $M_{\rm Jup}$) for this object. HD 19467 B is instead a fully evolved object with a $T_{\rm eff}$ of $\sim$1000 K and $\log g$ of $\sim$5.0 dex. Its spectral type is T6 $\pm$ 1.

Key words: instrumentation: spectrographs – methods: data analysis – techniques: imaging spectroscopy – infrared: planetary systems.

1 INTRODUCTION

Brown dwarfs (BDs) are low-mass objects populating the mass range between stars and planets. First theorized by Kumar (1963) and Hayashi & Nakano (1963), it was not until 1995 that the first unquestionable evidence of their existence was provided (Nakajima et al. 1995; Rebolo, Zapatero Osorio & Martín 1995). Because of their low mass, these objects are not capable to sustain hydrogen burning in their cores and they continuously cool down during their lifetime (Baraffe et al. 2003). The distinction between BDs and planets is conventionally set at the minimum mass for which deuterium (D) can fuse into ^{3}He nuclei. This value has been defined as the mass of objects able to burn the 90 per cent of their initial D in 10 Gyr and it was found to range from 13.1 to 12.4 $M_{\rm Jup}$, for cloudless and cloudy models, respectively (Saumon & Marley 2008). Furthermore, Spiegel, Burrows & Milsom (2011) found that this value is valid for objects at solar metallicity, while it varies from 11.0 $M_{\rm Jup}$ for a metallicity three times the solar value to 16.3 $M_{\rm Jup}$ for zero metallicity.

An alternative approach to distinguish between planets and BDs is through their formation mechanism. The detection of substellar objects in young stellar clusters (e.g. De Marchi, Paresce & Portegies Zwart 2010) and the fact that collapse formation scenarios foresee that the minimum fragment masses are well extended in the substellar regime (e.g. Vázquez-Semadeni et al. 2019) are clear hints that the formation through the fragmentation of molecular clouds is possible also for this type of objects. Alternatively, they could form following planet-like mechanisms like the gravitational instability (Cameron 1978) into protoplanetary discs. It is nowadays

★ E-mail: dino.mesa@inaf.it

© 2020 The Author(s)
Published by Oxford University Press on behalf of the Royal Astronomical Society

Downloaded from https://academic.oup.com/mnras/article/495/4/4279/5843294 by guest on 01 September 2023

recognized that these two formation mechanisms overlap on mass ranges of few Jupiter masses (Kiefer et al. 2019).

To clarify the nature of these objects, studies both in the visible (Cruz, Kirkpatrick & Burgasser 2009) and in the near-infrared (NIR; e.g. Allers et al. 2010; Seeliger, Neuhäuser & Eisenbeiss 2011; Allers & Liu 2013; Martin et al. 2017) were performed on field BDs. Observing these objects in the NIR is very important because a large fraction of the flux emitted by L and T dwarfs is at wavelengths ranging between 1 and 2.5 μm. In addition, the NIR spectrum of these objects contains a wealth of spectral features ranging from narrow atomic lines to broad molecular bands that have different dependencies on their temperature, gravity, and metallicity (Kirkpatrick 2005).

In recent years, new high-contrast imaging instruments like NACO (Lenzen et al. 2003), GPI (Macintosh et al. 2014), NICI (Chun et al. 2008), NIRI (Hodapp et al. 2003), NIRC2 (e.g. Mawet et al. 2017), and SPHERE (Beuzit et al. 2019) allowed to detect several BDs companions of main-sequence or pre-main-sequence stars (see e.g. Mawet et al. 2015; Konopacky et al. 2016; Milli et al. 2017; Cheetham et al. 2018). The possibility to study the spectral characteristics of these BD companions can provide additional, complementary information to observations of isolated, field BDs.

Currently, only a handful of BD companions has been spectroscopically investigated exploiting the limited resolution ($R \sim 30$–50) of integral-field spectrograph such as SPHERE and GPI. Some examples include HR 2562 B (Konopacky et al. 2016; Mesa et al. 2018), HD 984 B (Johnson-Groh et al. 2017), HD 1160 B (Maire et al. 2016; Garcia et al. 2017), HD 206893 B (Delorme et al. 2017), HD 4747 B (Crepp et al. 2018; Peretti et al. 2019), and HD 13724 B (Rickman et al. 2020). In only five more cases, it was possible to obtain a spectrum with a larger resolution ($R = 350$), using the SPHERE long-slit spectroscopy (LSS; Vigan et al. 2008) observing mode. This has been done for 2MASS J01225093−2439505 B (Hinkley et al. 2015), PZ Tel B (Maire et al. 2016), HR 3549 B (Mesa et al. 2016), HD 284149 B (Bonavita et al. 2017), and HIP 64892 B (Cheetham et al. 2018). Moreover, spectra in the NIR for companions at large separation from the host star were obtained at medium resolution (1500–2000) with SINFONI (e.g. Bonnefoy et al. 2014).

In this paper, we expand upon the current sample and we focus on two substellar objects orbiting the nearby stars HD 1160 and HD 19467. These systems are described in detail in Section 2. Furthermore, we present in Section 3 our data and the data reduction procedure adopted. In Section 4, we then present and discuss our main results. Finally, in Section 5 we give our conclusions.

2 TARGET PROPERTIES

HD 1160 is an A0V (Houk & Swift 1999) star at a distance of 125.9 ± 1.2 pc (Gaia Collaboration 2018). Around this star, Nielsen et al. (2012) detected two companions, HD 1160 B and HD 1160 C at separations of ∼80 and 530 au, respectively, using NICI at the Gemini telescope. They found a spectral type of L0 for HD 1160 B and a spectral type of M3.5 for HD 1160 C. They were also able to determine a mass in the range between 24 and 45 M_{Jup}, in the BDs regime, for the former and in the range between 0.18 and 0.25 $M_{\odot}$, in the stellar regime, for the latter assuming an age between 10 and 100 Myr.

HD 1160 was also observed with SPHERE in IRDIFS_EXT mode obtaining a low-resolution ($R = 30$) spectrum of HD 1160 B in the NIR between 0.95 and 1.65 μm (Maire et al. 2016). This allowed to re-classify its spectral type as M6 and to derive a $T_{\rm eff}$ of 3000 ± 100 K and a subsolar metallicity. However, they could not provide constraints on the surface gravity. They assumed a wider range for the age (30–300 Myr) resulting in masses between 39 and 166 M_{Jup}.

More recently, this system was studied through SCExAO and GPI by Garcia et al. (2017). They found for HD 1160 B $T_{\rm eff} = 3000$–3100 K and $\log g = 4$–4.5 dex, in agreement with the relatively young age of the system. Differently from Maire et al. (2016), they did not find evidence of subsolar metallicity, as expected according to standard Galactic chemical evolution models and observations (see e.g. Bensby, Feltzing & Oey 2014; Spina et al. 2017, and references therein). The authors also clearly stressed that the main uncertainty on the mass determination for this object is due to the estimation of the age of the system (for ages between 80 and 125 Myr, the mass of this object can vary from the BD regime to hydrogen-burning limit).

Recently, Curtis et al. (2019) assigned HD 1160 as a member of the recently discovered Pisces–Eridanus (Psc–Eri) stellar stream (Meingast, Alves & Fürnkranz 2019) exploiting kinematics. They also defined for the stream an age of 120 Myr, in fair agreement with the estimate of 135 Myr later found by Röser & Schilbach (2020). Should the membership of HD 1160 to the Psc-Eri stream be confirmed, the mass of HD 1160 B would be of the order of 0.12 $M_{\odot}$, well into the stellar mass range (Curtis et al. 2019).

HD 19467 is a G3 (Houk & Smith-Moore 1988) star at a distance of 32.02 ± 0.04 pc (Gaia Collaboration 2018). Using NIRC2 high-contrast imaging and HIRES radial velocity (RV) data, Crepp et al. (2014) detected a companion at a separation larger than 1.6 arcsec. Combining Doppler observations and imaging, they estimated a minimum mass just above 50 M_{Jup} for the companion. Moreover, they estimated an age of 4.3 Gyr through gyrochronology while isochrones provided an older age of 9 ± 1 Gyr. By adopting these ages and using K_s photometry, Crepp et al. (2014) obtained companion masses of 56.7 and 67.4 M_{Jup}, respectively. Finally, from the measured colours they inferred a T5–T7 spectral type.

HD 19467 was also observed using the Project 1640 instrument at the Palomar Observatory by Crepp et al. (2015). They extracted a low-resolution ($R \sim 30$) spectrum of HD 19467 B that allowed to define a spectral type of T5.5 ± 1 and a $T_{\rm eff}$ of 980 K.

Recently, Wood et al. (2019) estimated, through isochronal models, an age of $10.06^{+1.16}_{-0.82}$ Gyr for HD 19467, and found a mass of 67–69 M_{Jup} for HD 19467 B. Very recently, Maire et al. (2020) presented a thorough investigation of the host star properties and found for the system an age of $8.0^{+2.0}_{-1.0}$ Gyr. We will then assume in our work this age estimation for consistency with that paper.

3 OBSERVATIONS AND DATA REDUCTION

We observed HD 1160 and HD 19467 with the SPHERE IRDIS (Dohlen et al. 2008) scientific subsystem operating in the LSS medium resolution (MRS) observing mode. This mode allows to obtain spectra with a resolution of $R = 350$ covering the *Y*, *J*, and *H* spectral bands simultaneously for companions with contrasts of the order of 10^{-5} to 10^{-6} at separations larger than 0.5 arcsec.

We observed HD 1160 in the night of 2018 August 20 and HD 19467 in the night of 2019 January 26. Both these observations were obtained in service mode. In Table 1, we report the main informations regarding the two observing nights. In both nights, seeing and coherence time were stable along all the observations resulting in a stable Strehl ratio with values above 80 per cent. In the same table, we also listed the number of datacubes obtained for each observation together with the number of frames obtained

Downloaded from https://academic.oup.com/mnras/article/495/4/4279/5843294 by guest on 01 September 2023

Table 1. Characteristics of the SPHERE observations presented in this work. In column 1 we list the observing night, in column 2 we list the target name, and in column 3 we report the coronagraph used. In columns 4 and 5, we list the number of datacubes, the number of frames for each datacube, and the exposure time expressed in s for each frame for observation with the slit on (labelled Obs. comp.) and outside the companion position (labelled Obs. no comp.). In columns 6, 7, and 8, we report the median values of seeing, coherence time, and wind speed during the observations.

Date	Target	Coronagraph	Obs. comp.	Obs. no comp.	S (arcsec)	τ_0 (ms)	Wind (m s^{-1})
2018-08-20	HD 1160	N_S_MR_WL	5 × 9;32	5 × 8;32	0.49	4.6	11.10
2019-01-26	HD 19467	N_S_MR_WL	5 × 11;32	5 × 10;32	0.47	17.4	2.13

for each datacube and the exposure time for each frame. The total observing time on the target was of 24 min for HD 1160 and around 30 min for HD 19467. In both cases, we alternated observations with the slit on the position of the companion and observations with the slit rotated outside the position of the companion. This observing techniques was first proposed for the case of the SPHERE LSS observing mode in Vigan et al. (2016b) and its aim is to use the data with the slit outside the companion to create a reliable model of the speckle pattern to be subtracted from the data with the slit on the companion. All the data (i.e. with/without the companion into the slit) were taken with the host star behind the coronagraph. In order to properly calibrate the flux of the extracted spectrum of the companion, we also obtained a spectrum of the star outside the coronagraphic mask. Finally we observed, in the same configuration of the flux calibration data, one early-type star for each of our target just after the end of the scientific observations. They were then used to remove telluric lines and obtain a more accurate wavelength solution. To this aim, we observed the B8 star HD 225187 in the case of HD 1160 and the B3 star HD 20001 in the case of HD 19467.

We prepared a custom Python-based pipeline to reduce these data (detailed information will be provided in a forthcoming publication; Mesa et al., in preparation). As first step, master dark, bad pixels map, and master detector flat are produced. We then create the wavelength calibration file. The scientific data with the companion in the slit and those with the companion outside the slit are then reduced separately applying the appropriate calibrations and finely registering each frame. We also corrected a known problem of the MRS observing mode that, due to a slight tilt (∼1 degree) of the grism on its mount, produce a different position of the companion point spread function (PSF) at different wavelengths. The reduced data without the companion were then used to create a model of the speckle pattern using a procedure based on the principal components analysis (PCA; Soummer, Pueyo & Larkin 2012). This model was then subtracted from each frame of the data set with the companion into the slit to effectively subtract the speckle pattern from them and to improve the signal to noise ratio (SNR) of the extracted spectrum that is composed by 780 wavelengths ranging between 0.94 and 1.82 μm. For the spectral extraction, we used a fixed extraction window following the method devised in Bonavita et al. (2017). The uncertainties on the extracted spectrum were obtained calculating the standard deviation on a window defined in the same way of that used for the spectrum extraction. Moreover, this window was at the same separation of the companion but on the opposite side with respect to the host star. We extracted also the spectra of the host star and of the standard star following the same method used for the companion. We then finely recalibrated the wavelengths of the companion and of the host star spectra using as reference the positions of the telluric lines found in the standard star. Finally, we obtained the spectrum of the companion in contrast dividing it by the spectrum of the host star.

With the aim to check the reliability of our results, we also reduce our data using the SILSS pipeline (Vigan 2016) that is purposely designed to reduce SPHERE LSS data sets. Both for HD 1160 and for HD 19467, the extracted spectra with the two pipelines were in good agreement confirming the reliability of our results. To quantify the agreement between the two methods, we calculated the differences between the two spectra and we verified that, for each wavelength, this is smaller than the uncertainties.

4 RESULTS AND DISCUSSION

4.1 HD 1160 B

The contrast spectrum of the companion extracted following the method described in Section 3 is transformed in flux multiplying it for an appropriate BT-NEXTGEN (Allard, Homeier & Freytag 2012) theoretical spectrum, following a standard procedure previously used in other works of our group (e.g. Maire et al. 2016; Vigan et al. 2016a; Zurlo et al. 2016; Bonavita et al. 2017; Mesa et al. 2018). To identify the appropriate model spectrum, we used the VOSA SED analyser[1] (Bayo et al. 2008) to find the model with the best fit with the stellar spectral energy distribution (SED). At the end of this procedure, we selected a model with $T_{\rm eff} = 9200$ K, surface gravity $\log g = 4.5$ dex, and solar metallicity.

The spectrum resulting from this procedure was very noisy for the lower and for the higher wavelengths and for this reason we excluded all the wavelengths below 0.97 μm and above 1.80 μm. Furthermore, we excluded also all the wavelengths in the spectral region around 1.4 μm that are affected by the presence of water telluric absorption. At the end of this procedure, we remained with a spectrum composed of 658 data points that is shown in Fig. 1.

From the extracted spectrum, we obtained the photometric values for Y (wavelengths below 1.15 μm), J (wavelengths between 1.15 and 1.4 μm), and H (wavelengths above 1.4 μm) spectral bands that are listed in the second column of Table 2. Thanks to these values and exploiting the BT-Settl models (Allard 2014), we estimated the mass of the companion. To this aim, we adopted both a young system age of 50^{+50}_{-40} Myr as proposed by Nielsen et al. (2012) and the older age of ∼120 Myr proposed by Curtis et al. (2019). In this second case, as an error on the age was not given by Curtis et al. (2019), we considered an uncertainty of 15 Myr using also the age determination from Röser & Schilbach (2020) for the Psc-Eri stellar stream. The results of this procedure are listed in the second and the third column of Table 3. In the first case (i.e. young age), the uncertainties on the mass are very large mainly due to the large uncertainties on the system age, so that masses encompass the low-mass brown dwarfs/stellar regime. As for the old age, the

[1] http://svo2.cab.inta-csic.es/theory/vosa/

Downloaded from https://academic.oup.com/mnras/article/495/4/4279/5843294 by guest on 01 September 2023

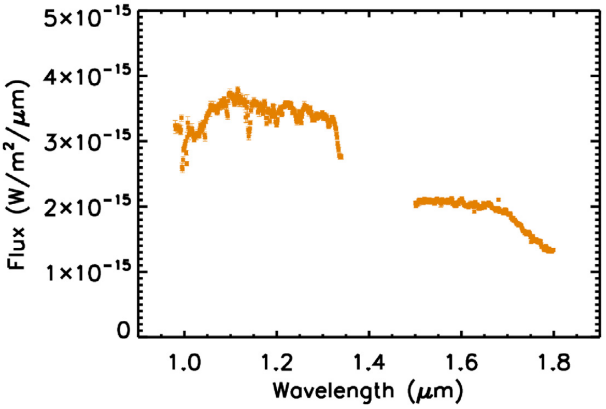

Figure 1. Spectrum for HD 1160 B extracted using the method described in Section 4.1.

Table 2. Absolute magnitude in *Y*, *J*, and *H* bands for HD 1160 (second column) and HD 19467 (third column).

Sp. band	Abs. mag. (HD 1160)	Abs. mag. (HD 19467)
Y	9.92 ± 0.01	16.39 ± 0.07
J	9.37 ± 0.01	15.13 ± 0.07
H	9.01 ± 0.01	15.84 ± 0.08

companion would be in the low-mass star regime, although at lower masses than those estimated by Curtis et al. (2019).

The spectral type of HD 1160 B is obtained by fitting its extracted spectrum with a sample of template spectra of field BDs taken from the *Montreal Brown Dwarf and Exoplanet Spectral Library*.[2] To construct this sample, we have considered only objects for which spectra with a resolution higher than that of the LSS mode of SPHERE were available. The spectra were then convolved with a Gaussian PSF to reduce the resolution to the same value of the LSS spectra. Finally, we interpolated the flux values to the same wavelengths of the LSS spectrum.

The best fit from this procedure is with the spectrum of 2MASSJ0805+2505 B, an M5 spectral type field dwarf (Gagné et al. 2015). Fits of comparable quality were also obtained for template spectra with spectral types M6 and M7 as shown in Fig. 2 where we also display the spectrum of 2MASSJ1358+0046 an M5.5 spectral type (Gagné et al. 2015) and of the M7 spectral type object 2MASSJ0518−3101 (Gagné et al. 2015). We can then conclude that the spectral type for HD 1160 B is M6 ± 1.

However, it is important to note that the quality of the fits, as highlighted by the value of the reduced χ^2 is not good for any of the template spectra. Indeed, none of them was able to produce a good fit both for the *Y*+*J* and the *H* spectral bands. This result is not completely surprising as similar difficulties to find a good fit with template spectra was experienced also by Maire et al. (2016) as can be seen from fig. 12 in that paper. Moreover, if we consider separately a fit for the two spectral bands, we find that while the first one tends to favour later (M7 ± 1) spectral types, the latter favours later spectral types (M5 ± 1). In the second case, the best fit is still with the M5 object 2MASSJ0805+2505 B while in the first case the best fit is obtained with the M7 spectral type 2MASSJ0518−3101.

To further confirm this result, we also display in Fig. 3 the distributions of the χ^2 values with respect to the spectral type of the fitting template spectra both for the *Y*+*J* bands and the *H* band. As highlighted by the two vertical lines, it is apparent that the two distributions have two different minimum at ∼M7 and ∼M5, respectively. While this difference is not large, it is however an indication that HD 1160 B has a peculiar spectrum.

An alternative way to classify the spectral type of this substellar object is to use spectral indices. To this aim, we have used the indices described in Allers & Liu (2013) that are fitted to the wavelength band of our observations. It is important to stress that these indices were thought for spectra at resolution slightly higher (∼700) than that used in our analysis. While these results should be then taken with care, they can however give a good indication of the spectral type of HD 1160 B. In particular, we used the H_2O index (Allers et al. 2007) that is effective for spectral types between M5 and L4 with an rms of 0.390 in spectral type and the H_2O-1 index (Slesnick, Hillenbrand & Carpenter 2004) that is effective for spectral types between M4 and L5 but with a larger rms of 1.097. The H_2O index, that is based on *H*-band wavelengths gives a spectral index of M4.8 while the H_2O index, that based on *J*-band wavelengths gives a later spectral type of M6.

These results confirm what we found with the fit with spectral templates and are a further indication of the peculiarity of the spectrum of HD 1160 B. The reasons of this peculiarity are not completely clear but we can do the hypothesis that it could be due to the presence of dust in its photosphere or to its young age (few tens of Myr). The second possibility would imply a still not fully evolved object explaining its peculiar spectrum. The presence of dust is in conflict with the high $T_{\rm eff}$ found for this object while the young age is in disagreement with the age of ∼120 Myr for the HD 1160 system proposed by Curtis et al. (2019).

With the aim to better define the physical characteristics of HD 1160 B, we also fitted the extracted spectrum to a grid of BT-Settl atmospheric models (Allard 2014) with a $T_{\rm eff}$ ranging between 900 and 4000 K with a step of 100 K, with $\log g$ ranging between 0.0 and 6.0 dex with a step of 0.5 dex and a solar metallicity following what previously found for this object by Garcia et al. (2017). The results of this procedure are displayed in Fig. 4 where the extracted spectrum of HD 1160 B is compared with the three best-fitting models. The best fit is obtained for a model with a $T_{\rm eff}$ of 2800 K and a surface gravity of $\log g = 3.5$ dex but comparably good fits are obtained for $T_{\rm eff}$ of 2900 K and a surface gravity of 3.5–4.0 dex. From this analysis we conclude that HD 1160 B has $T_{\rm eff} = 2800$–2900 K and $\log g = 3.5$–4.0 dex. This $T_{\rm eff}$ is in good agreement with the spectral classification of M7 found through the comparison with the *Y*+*J*-band spectral templates (Pecaut & Mamajek 2016).

Like for the case of the fit with the template spectra, we note that it is not possible to obtain a completely satisfactory fit between the extracted spectrum and the atmospheric models. This is a further indication that the spectrum of HD 1160 B is peculiar and that its classification is difficult. Also in this case, possible explanations are the presence of dust and/or the youth of the system.

To further constrain the gravity of HD 1160 B, we considered the alkali lines (Na I at 1.14 μm and K I doublets at ∼1.17 and ∼1.25 μm) that, for a given $T_{\rm eff}$, tend to become weaker at lower gravity (e.g. Gorlova et al. 2003; Cushing, Rayner & Vacca 2005). To this aim we have fitted the *J*-band (between 1.10 and 1.30 μm) spectrum of HD 1160 B with the atmospheric models with a fixed $T_{\rm eff}$ of 2800 K. In Fig. 5, we show how the value of χ^2 varies with $\log g$. The best fit is obtained for $\log g$ of 3.5–4.0 dex confirming what we found with the fit on the whole spectrum and with different $T_{\rm eff}$.

[2] https://jgagneastro.com/the-montreal-spectral-library/

Downloaded from https://academic.oup.com/mnras/article/495/4/4279/5843294 by guest on 01 September 2023

Table 3. Mass estimates in *Y*, *J*, and *H* bands for HD 1160 B considering the younger ages proposed by Nielsen et al. (2012) (second column – labelled as YA in the Table), for HD 1160 B considering the older age proposed by Curtis et al. (2019) (third column – labelled as OA in the table) and HD 19467 (fourth column).

Sp. band	Mass (HD 1160 B – YA) (M_{Jup})	Mass (HD 1160 B – OA) (M_{Jup})	Mass (HD 19467 B) (M_{Jup})
Y	$70.3^{+27.5}_{-47.2}$	$106.0^{+6.1}_{-6.4}$	$64.1^{+2.0}_{-2.4}$
J	$70.4^{+28.0}_{-49.4}$	$107.5^{+6.7}_{-7.1}$	$66.4^{+2.1}_{-1.9}$
H	$62.8^{+25.2}_{-42.6}$	$96.2^{+4.8}_{-6.3}$	$62.2^{+2.5}_{-3.5}$

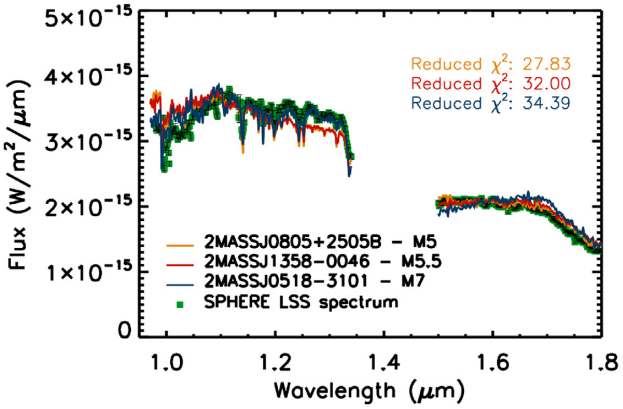

Figure 2. Comparison of the extracted spectrum for HD 1160 B (green squares) with the three best-fitting spectra from the Montreal library (red, orange, and blue solid lines).

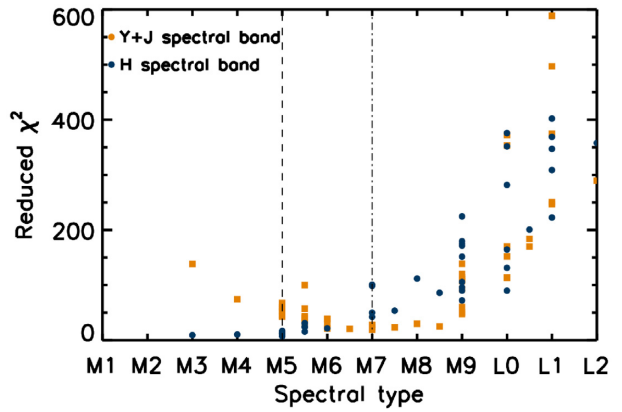

Figure 3. Values of the χ^2 obtained from the fit versus the spectral type of the template spectra. The orange squares represent the values obtained using only the *Y*+*J* spectral bands, the blue circles represent the values obtained using the H spectral band. The dashed vertical line highlights the position of the minimum for the *H*-band distribution, the dot–dashed line is the same thing for the *Y*+*J*-band distribution.

Furthermore, we tested the gravity sensitive spectral index linked to the Na I line at 1.14 μm defined in Allers et al. (2007) for spectra with a resolution of the order of 300 similar to that of our data. We obtained for this index a value of 1.08 that indicates low gravity. This index is however reliable only for spectral types later than M6 so that our target is at the edge of the validity range of this index. We also calculated the KIJ index defined in Allers & Liu (2013) obtaining a value of 1.032 that is coherent with an intermediate value for the surface gravity. From all these results, we can then

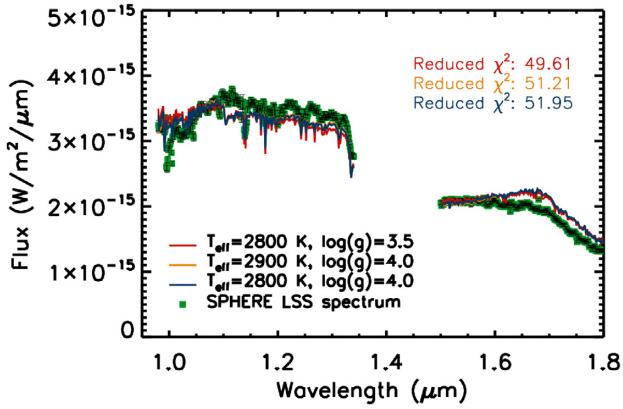

Figure 4. Comparison of the extracted spectrum for HD 1160 B (green squares) with the three best-fitting theoretical BT-Settl spectra (orange, red, and blue solid lines).

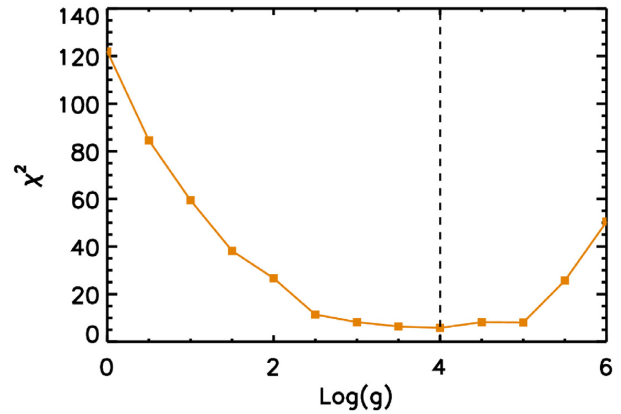

Figure 5. Values of the χ^2 obtained from the fit versus the values of log *g* for a fixed $T_{\rm eff}$ of 2800 K. The vertical dashed line highlights the position of the minimum of the curve.

conclude that HD 1160 B is an intermediate gravity object with a log *g* of 3.5–4.0 dex.

Also, in this case, our results are not in agreement with an age of the system of the order of 120 Myr and a mass of 0.1 $M_\odot$ as proposed by Curtis et al. (2019). Indeed, according to the BT-Settl models, an object with such mass and age would require a log *g* of the order of 5.0 dex. To match the values of log *g* deduced from our analysis, we would instead need an object at the younger end (10–20 Myr) of the age range proposed by Nielsen et al. (2012) and as a consequence, the lower mass in the range calculated in Table 3 (around 20 M_{Jup}).

Using the wide-band photometry listed in Table 2 we produced, following the procedure described in Bonnefoy et al. (2018), the

Downloaded from https://academic.oup.com/mnras/article/495/4/4279/5843294 by guest on 01 September 2023

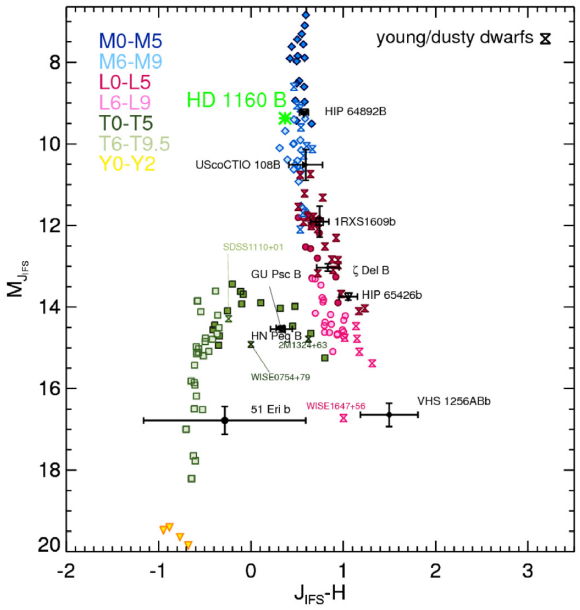

Figure 6. Absolute *J* magnitude versus *J–H* colour–magnitude diagram with the position of HD 1160 B that is indicated by a green asterisk. The positions of field M, L, and T dwarfs are also represented in different colours according to the spectral type. Black asterisk represents the positions of other substellar companions.

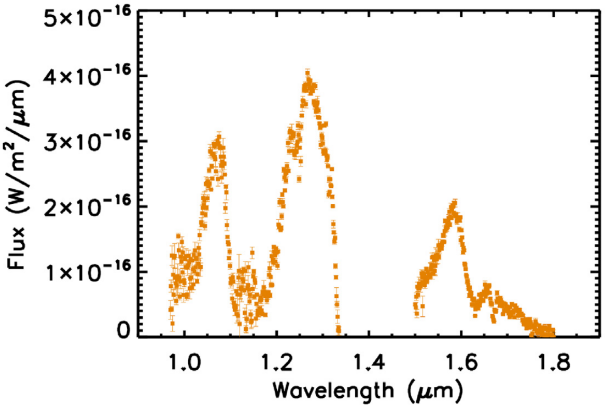

Figure 7. Extracted spectrum for HD 19467 B using the method described in Section 4.2.

absolute *J* magnitude versus *J–H* colour–magnitude diagram that is displayed in Fig. 6. The position of HD 1160 B, indicated by a green asterisk, is compared to those of M, L, and T field dwarfs indicated in different colours according to the spectral type and to other substellar companions indicated by black asterisks. Its position is coherent with that of medium M spectral type objects confirming what we found with previous analysis.

4.2 HD 19467 B

Following the same procedure used for HD 1160 B, we transformed the contrast spectrum of HD 19467 B into the flux spectrum displayed in Fig. 7. In this case, the BT-Nextgen synthetic model with the best fit to the stellar SED and used for this procedure was that with $T_{\rm eff}$ = 5600 K, a surface gravity with $\log g$ = 4.5 dex and solar metallicity. As for HD 1160 B, we also used the extracted

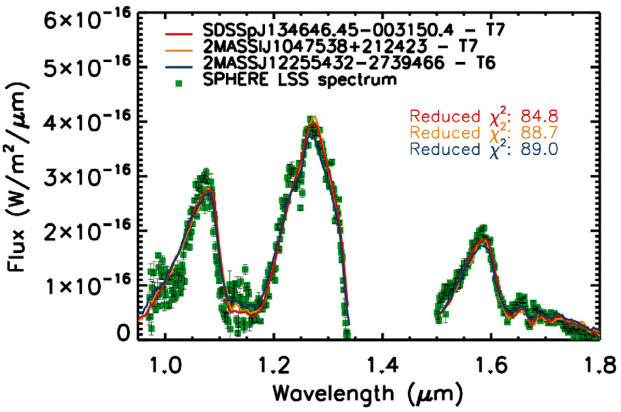

Figure 8. Comparison of the extracted spectrum for HD 19467 B (green squares) with the three best-fitting spectra from the *SpexPrism* library (red, orange, and blue solid lines).

spectrum to calculate the absolute magnitude and to estimate the mass of the companion. To this aim we adopted the system age of $8.0^{+2.0}_{-1}$ Gyr as mentioned in Section 2. Because the magnitude of HD 19467 B is outside the range covered by the BT-Settl models, we employed the AMES-Cond grid of atmospheric models (Allard et al. 2003). The values resulting from this procedure are listed in the third column of Table 2 and in the fourth column of Table 3. In this case, the uncertainties are small and the mass ranges between 60 and 68 $M_{\rm Jup}$, compatible to what found by Wood et al. (2019).

We followed for HD 19467 B the same procedure used for HD 1160 B comparing its spectrum with those of template spectra. In this case, however, we were not able to find a large library of high-resolution spectra in the T spectral type regime. For this reason we used the lower resolution spectra in the *Spex Prism spectral libraries*[3] (Burgasser 2014). This will not allow to exploit the full potential of the spectral lines in the spectral classification but will however allow to perform a reliable definition of the spectral type. The results of this procedure are displayed in Fig. 8 where the LSS extracted spectrum is compared to the three best-fitting spectra. In this case, the best fit is obtained with the T7 spectrum of SDSSp J134646.45−003150.4 (Burgasser, Burrows & Kirkpatrick 2006) but a comparable good fit is obtained for spectra with spectral type between T5 and T7. For this reason, we can conclude that the spectral type for this object is T6 ± 1.

As done for HD 1160 B, we have tried to confirm this spectral classification calculating appropriate spectral indices. To this aim we have used the H_2O index at 1.15 μm, the H_2O index at 1.5 μm and the CH_4 index at 1.6 μm defined by Geballe et al. (2002). The first index is accurate only for subtyping in the T sequence, the second one is reliable both on the L and T sequences while the third one is again effective for the T sequence. We found for these three indices values of 6.35, 5.56, and 3.13, respectively, for the case of HD 19467 B. According to the values for the L–T dwarfs subtyping listed in table 5 of Geballe et al. (2002), these values are coherent with a T6 spectral type. This is in good agreement with the spectral type defined through the comparison with template spectra.

Similarly to the case of HD 1160 B, we have fitted also the extracted spectrum of HD 19467 B with a grid of BT-Settl atmospheric

[3]http://pono.ucsd.edu/~adam/browndwarfs/spexprism/

Downloaded from https://academic.oup.com/mnras/article/495/4/4279/5843294 by guest on 01 September 2023

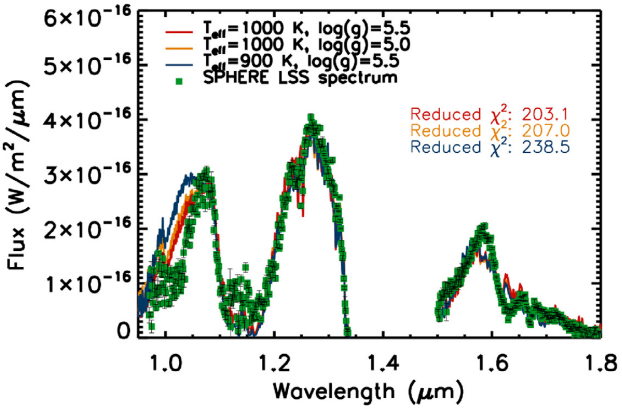

Figure 9. Comparison of the extracted spectrum for HD 19467 B (green squares) with the three best-fitting theoretical BT-Settl spectra (orange, red, and blue solid lines).

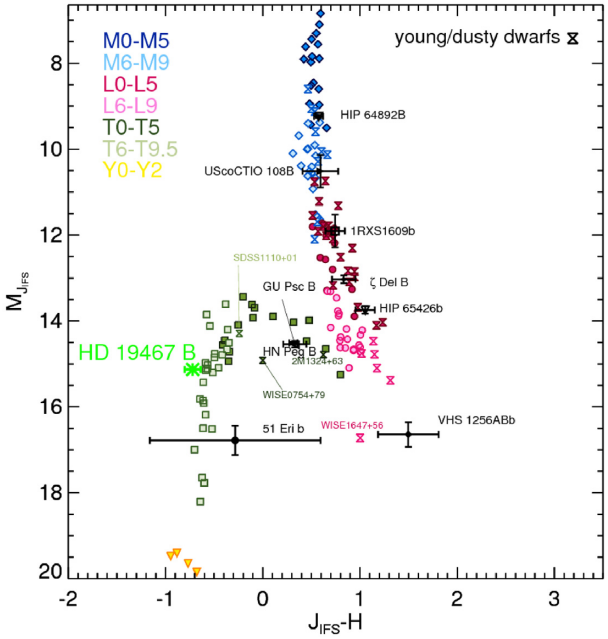

Figure 10. Absolute J magnitude versus J–H colour–magnitude diagram with the position of HD 19467 B that is indicated by a green asterisk. The positions of field M, L, and T dwarfs are also represented in different colours according to the spectral type. Black asterisks represent the positions of other substellar companions.

models. In this case, their $T_{\rm eff}$ ranges between 500 and 2500 K with a step of 100 K, the surface gravity ranges between 2.5 and 5.5 dex while we used solar metallicity models. The results of this procedure are displayed in Fig. 9 where we compare the extracted spectrum with the three best-fitting models. The best-fitting model is obtained for a $T_{\rm eff}$ of 1000 K and a log g of 5.5 dex. Good fits were however obtained also for $T_{\rm eff}$ between 900 and 1100 K while the surface gravity is generally higher than 4.5 dex. From these results, we can conclude that HD 19467 B has $T_{\rm eff} = 1000 \pm 100$ K and $\log g = 5.0 \pm 0.5$ dex. In this case, the $T_{\rm eff}$ obtained is in good agreement with what foreseen by Pecaut & Mamajek (2016) for the spectral type that we derived previously for this object.

Following the procedure used for HD 1160 B, we have created also for HD 19467 B an absolute J magnitude versus J–H colour–magnitude diagram (see Fig. 10). In this diagram, the position of this object is in good agreement with the expected positions of medium T spectral type objects.

4.2.1 Atmospheric retrieval of HD 19467 B

In this section, we use the extracted spectrum of HD 19467 B to perform a retrieval analysis in order to obtain a more in-depth insight into the physical and chemical properties of HD 19467 B. For the retrieval, we use the Bayesian, nested-sampling retrieval model `Helios-r2` (Kitzmann 2020).[4] The model and its application to emission spectra of brown dwarfs is extensively discussed in Kitzmann et al. (2020).

Besides the surface gravity log g, the calibration factor f, and the distance d, we retrieve the abundances of H_2O, CH_4, K, and Na. We also tried to include the mixing ratios of NH_3, CO, and CO_2, which led to unconstrained, prior-dominated posterior distributions. We, therefore, omit these molecules in the final analysis. For the distance d, we use a Gaussian prior with a mean value of 32.02 pc and a standard deviation of 0.04 pc, based on GAIA parallax measurements. The temperature profile is described by six first-order elements (see Kitzmann et al. 2020, for details on the parametrization of the temperature profile). We also add a grey cloud layer to the retrieval, determined by three parameters (cloud top pressure, the bottom of the cloud layer, defined as a multiplicative factor of the cloud top pressure, and the grey optical depth). The a priori brown dwarf radius is assumed to be 1 $R_{\rm Jup}$. Any deviations from this assumed radius are contained in the calibration factor f. In total, we used 18 free parameters, including the parameter aimed to the inflation of the observational errors following the method described by Line et al. (2015) and Kitzmann et al. (2020). The inflation of the errors is used to take into account the fact that the simplified physical model used here is usually not able to describe all the details in a measured brown dwarf spectrum.

Note that for this retrieval we cut the spectrum below 1.2 μm. This is necessary to obtain physically consistent values for the surface gravity and the calibration factor. The direct retrieval of the surface gravity and the brown dwarf radius from medium-resolution emission spectra is known to be problematic (e.g. Kitzmann et al. 2020; Oreshenko et al. 2020). The spectrum around 1 μm, which is dominated by the alkali resonance line wings, plays an important role in the determination of log g. Inaccuracies in the measured data, but also the theoretical description of the line wings can strongly influence the retrieved values of the surface gravity. We, therefore, did not use this problematic region for the spectral retrieval. However, for comparison, we add a retrieval using the entire available spectral range in the Appendix.

The resulting posterior distributions are shown in Fig. 11, while derived quantities and the posterior spectra are presented in Fig. 12. The retrieved values for the surface gravity log g are quite high, while the calibration factor f is smaller than unity. On the other hand, the obtained value of $\log g = 5.44 \pm 0.05$ dex is within the confidence interval of the estimates based on the BT-Settl models, where a value of 5 ± 0.5 dex is found (see Section 4.2). By assuming that f only describes deviations with

[4] `Helios-r2` is available as open-source software on the Exoclimes Simulation Platform (ESP) (http://www.exoclime.org/).

Downloaded from https://academic.oup.com/mnras/article/495/4/4279/5843294 by guest on 01 September 2023

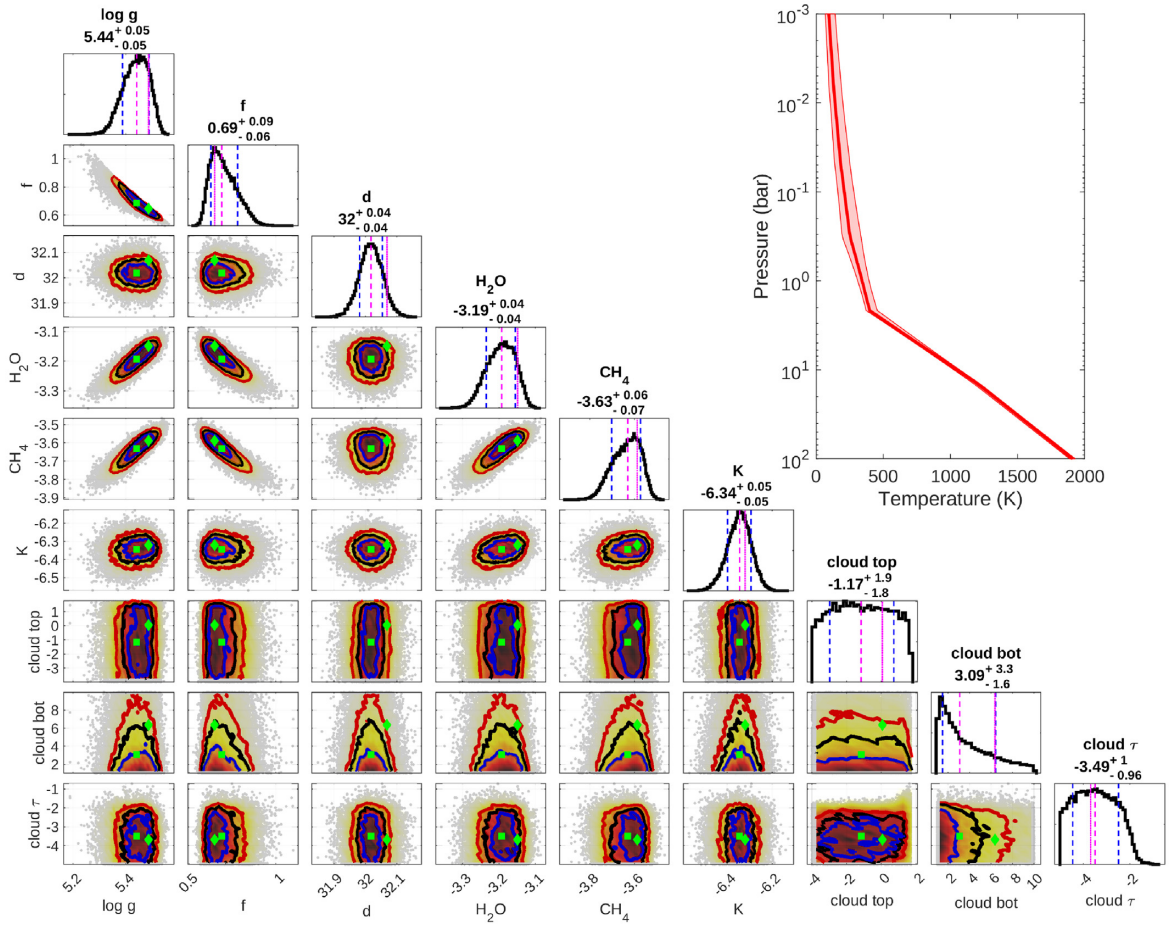

Figure 11. Posterior distributions for the retrieval of HD 19467 B. The dashed magenta-coloured lines in the posterior plots refer to the location of the median value (also stated below each parameter), while the 1σ confidence limit is denoted by the blue dashed lines. The magenta dotted line shows the location of the best-fitting model, i.e. the one with highest likelihood value. The solid blue, red, and yellow lines in the two-dimensional parameter correlation plots mark the 1σ, 2σ, and 3σ intervals, respectively. Here, the location of the median (best-fitting) model is marked by green squares (diamonds). The panel in the upper, right corner depicts the retrieved temperature profile. The solid red line corresponds to the median profile, while the shaded, red area corresponds to the 1σ confidence interval.

respect to assumed radius of 1 R_{Jup}, it can be converted into a posterior for the brown dwarf radius, shown in Fig. 12. In reality, however, f also includes other sources of errors, for example, inaccuracies in the calibration of the spectrum, systematic errors of the instruments and detector, or errors in the distance measurements. The retrieved value for f of 0.69 ± 0.09 results in a radius estimate of 0.83 ± 0.06 R_{Jup}, which is consistent with evolutionary calculations by Saumon & Marley (2008) for such an old object.

The retrieved abundances of H_2O, CH_4, and K are all well constrained. As mentioned above, adding NH_3, CO, and CO_2 as free parameters will result in unconstrained, prior-dominated posterior distributions. Based on the retrieved abundances, we estimate the C/O ratio and metallicity in Fig. 12. Both, the C/O ratio and the overall metallicity are subsolar. Within its confidence intervals, this is consistent with the values found for the host star (Maire et al. 2020). We note, however, that both quantities are only estimates based on the H_2O, CH_4, and K values (H_2 and He are assumed to form the background of the atmosphere) and that other molecules that are not detected in the available part of the spectrum might change these estimates.

All cloud parameters are essentially unconstrained which suggests that the presence of a grey cloud layer is not favoured by the data. The temperature profile, on the other hand, is well constrained as evidenced by the small uncertainties shown by the shaded area in the right-hand panel of Fig. 11.

The effective temperature presented in Fig. 12 has been obtained by integrating the posterior spectra over wavelengths and converting the flux to an effective temperature using the Stefan–Boltzmann law. Its value of about 900 K agrees well with the estimates derived from BT-Settl models (see Section 4.2).

Due to the small radius and high surface gravity, the derived mass shown in Fig. 12 is also quite large. The obtained value of $78^{+1.6}_{-3.1}$ M_J is almost at the edge of the usually assumed upper mass limit for brown dwarfs ($80\,M_J$). As can be seen in Fig. 12, the posterior distribution is also cut at higher masses. Within the retrieval, we reject all masses larger than $80\,M_J$ to not allow the nested sampling to move into an unrealistic mass regime. Without that cut-off, the retrieved mass would even be a bit higher than the value we obtain here.

The posterior spectra shown on the bottom panel of Fig. 12 suggest that overall the retrieval matches the measured spectrum

Downloaded from https://academic.oup.com/mnras/article/495/4/4279/5843294 by guest on 01 September 2023

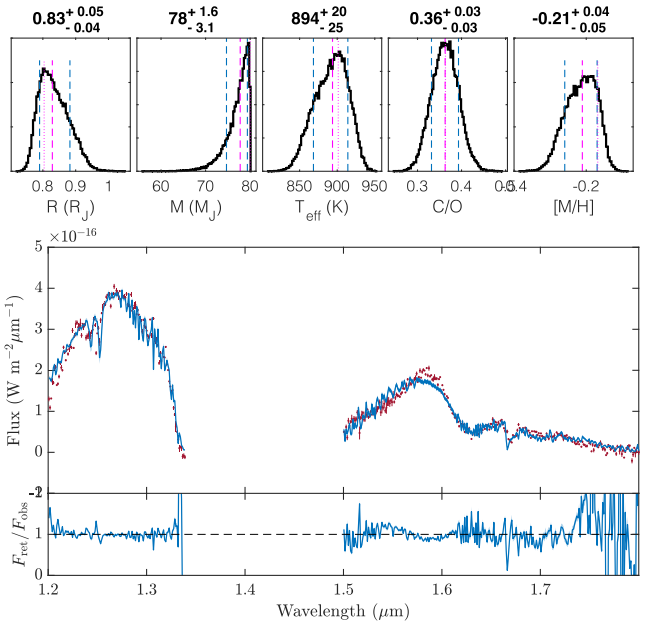

Figure 12. *Top*: Posterior distributions of derived quantities for the retrieval of HD 19467 B. The posteriors are shown for the brown dwarf radius R, its mass M, effective temperature $T_{\rm eff}$, the C/O ratio, and the overall metallicity [M/H]. *Bottom*: Posterior spectra and residuals. The solid lines refer to the median of all posterior spectra. The shaded areas signify the 3σ confidence intervals of the spectra. The measured spectrum is indicated by the red data points.

quite well. Notable discrepancies are found in the red part of the spectrum. Here, we underestimate the peak in the flux near 1.55 μm, whereas at the red edge, we slightly overestimate the continuum flux. This might be caused by an additional molecular absorber that has not been included in the retrieval.

5 SUMMARY AND CONCLUDING REMARKS

We presented in this paper SPHERE LSS mode observations of the two benchmark brown-dwarf companions HD 1160 B and HD 19467 B. The high-quality (SNR and resolution) spectra for these two objects allowed us to obtain a precise spectral calibration and to gather information on their main physical properties.

For the case of HD 1160 B, the main source of the errors on its physical parameters is due to the large uncertainty on its age. This is important in the derivation of its mass. We have assumed here a range between 10 and 100 Myr that leads to a mass ranging between low-mass brown dwarfs to the low-mass stars regime. We also tested an older age of ∼120 Myr, recently proposed for the HD 1160 system that results in a low-star mass for HD 1160 B. The comparison with template spectra gives the best fit with M6 ± 1 spectral types. Anyway our procedure is not able to obtain satisfactory fits both in the Y+J and the H spectral band, simultaneously. Indeed, performing a fit separately in the Y+J and the H spectral bands tends to favour later and earlier spectral types, respectively. This dichotomy was also confirmed by the two spectral indices linked to the H_2O molecule, the first in the J band and the second in the H band. We conclude that the HD 1160 B spectrum is very peculiar given that it is not possible to find a similar spectrum in the currently available spectral libraries. This could be due to a young age of the system and/or to the presence of dust in the photosphere of this object.

We also compared the spectrum to BT-Settl atmospheric models and we found that the best fit is obtained for models with $T_{\rm eff}$ of 2800–2900 K and a surface gravity of $\log g = 3.5$–4.0 dex. Using only the spectral region between 1.10 and 1.30 μm that contains important alkali (Na I and K I) lines that are good indicators of the surface gravity allows us to further confirm the value found previously. Moreover, an intermediate value for the surface gravity is also confirmed using apposite spectral indices.

This last result has an important consequence on the age (and then on the mass) of HD 1160 B. Indeed according to the atmospheric models, a stellar mass for this object, implied if we assume the older ages (120 Myr) proposed for the system, would require a surface gravity of the order of 5.0 dex that seems to be ruled out by our analysis. Instead, the surface gravity that we have defined for this object favour the younger ages (10–20 Myr) and lower masses (around 20 $M_{\rm Jup}$) in the proposed ranges. In any case, uncertainties on the fit with the models and in the determination of the spectral indices do not allow to fully exclude the possibility of an older age. Further analysis at higher spectral resolution and with different instruments will be necessary to completely solve these uncertainties.

HD 19467 B is instead an old object and its mass can be defined with small uncertainties confirming that it is at the edge between the brown dwarfs and the low stellar mass regimes. We derived a T6 spectral type, through the comparison with templates and using apposite spectral indices. This is in good agreement with the $T_{\rm eff}$ of the order of ≈1000 K that we found from the comparison of its spectrum with BT-Settl atmospheric models. Finally, we derived a large value for the surface gravity ($\log g = 5.0$ dex) that confirms the old age of this fully evolved object.

Finally, we performed on the latter object spectral retrieval to further define its physical and chemical characteristics. $T_{\rm eff}$ and surface gravity were in good agreement with what we found using the evolutive models while the mass of the object tends to be higher than what we found with the models. From the point of view of the chemical abundances, we were able to put strong constraints on the abundances of H_2O, CH_4, and K while this was not possible for other molecules like NH_3, CO, and CO_2. Furthermore, our analysis does not favour the presence in the atmosphere of this object of a grey cloud layer.

It was not possible to apply the spectral retrieval analysis to the case of HD 1160 B due to the fact that these models are at the moment optimized to the case of cold objects and require to be adapted for the case of higher $T_{\rm eff}$. We defer this to a future work.

ACKNOWLEDGEMENTS

SPHERE is an instrument designed and built by a consortium consisting of IPAG (Grenoble, France), MPIA (Heidelberg, Germany), LAM (Marseille, France), LESIA (Paris, France), Laboratoire Lagrange (Nice, France), INAF-Osservatorio di Padova (Italy), Observatoire de Genéve (Switzerland), ETH Zurich (Switzerland), NOVA (Netherlands), ONERA (France), and ASTRON (Netherlands) in collaboration with ESO. SPHERE was funded by ESO, with additional contributions from CNRS (France), MPIA (Germany), INAF (Italy), FINES (Switzerland), and NOVA (Netherlands). SPHERE also received funding from the European Commission

Downloaded from https://academic.oup.com/mnras/article/495/4/4279/5843294 by guest on 01 September 2023

Sixth and Seventh Framework Programmes as part of the Optical Infrared Coordination Network for Astronomy (OPTICON) under grant number RII3-Ct-2004-001566 for FP6 (2004–2008), grant number 226604 for FP7 (2009–2012), and grant number 312430 for FP7 (2013–2016). We also acknowledge financial support from the Programme National de Planétologie (PNP) and the Programme National de Physique Stellaire (PNPS) of CNRS-INSU in France. This work has also been supported by a grant from the French Labex OSUG@2020 (Investissements d'avenir – ANR10 LABX56). The project is supported by CNRS, by the Agence Nationale de la Recherche (ANR-14-CE33-0018). It has also been carried out within the frame of the National Centre for Competence in Research PlanetS supported by the Swiss National Science Foundation (SNSF).

This research has made use of the SIMBAD database, operated at CDS, Strasbourg, France.

This research has benefited from the Montreal Brown Dwarf and Exoplanet Spectral Library, maintained by Jonathan Gagn'e.

This publication makes use of VOSA, developed under the Spanish Virtual Observatory project supported by the Spanish MINECO through grant AyA2017-84089. VOSA has been partially updated by using funding from the European Union's Horizon 2020 Research and Innovation Programme, under Grant Agreement no. 776403 (EXOPLANETS-A).

DM, VDO, RG, and SD acknowledge support from the 'Progetti Premiali' funding scheme of the Italian Ministry of Education, University, and Research.

DK acknowledges partial financial support from the Center for Space and Habitability (CSH) of the University of Bern and the PlanetS National Center of Competence in Research (NCCR).

This study is based on the observations collected at the European Organisation for Astronomical Research in the Southern Hemisphere under ESO programme 102.C-0191(A).

REFERENCES

Allard F., 2014, in Booth M., Matthews B. C., Graham J. R., eds, Proc. IAU Symp. Vol. 299, Exploring the Formation and Evolution of Planetary Systems. p. 271
Allard F., Guillot T., Ludwig H.-G., Hauschildt P. H., Schweitzer A., Alexander D. R., Ferguson J. W., 2003, in Martín E., ed., Proc. IAU Symp. Vol. 211, Brown Dwarfs. Astronomical Society of the Pacific, San Francisco, p. 325
Allard F., Homeier D., Freytag B., 2012, Phil. Trans. R. Soc. A, 370, 2765
Allers K. N., Liu M. C., 2013, ApJ, 772, 79
Allers K. N.e et al., 2007, ApJ, 657, 511
Allers K. N., Liu M. C., Dupuy T. J., Cushing M. C., 2010, ApJ, 715, 561
Baraffe I., Chabrier G., Barman T. S., Allard F., Hauschildt P. H., 2003, A&A, 402, 701
Bayo A., Rodrigo C., Barrado Y Navascués D., Solano E., Gutièrrez R., Morales-Calderon M., Allard F., 2008, A&A, 492, 277
Bensby T., Feltzing S., Oey M. S., 2014, A&A, 562, A71
Beuzit J. L. et al., 2019, A&A, 631, A155
Bonavita M. et al., 2017, A&A, 608, A106
Bonnefoy M., Chauvin G., Lagrange A. M., Rojo P., Allard F., Pinte C., Dumas C., Homeier D., 2014, A&A, 562, A127
Bonnefoy M. et al., 2018, A&A, 618, A63
Burgasser A. J., 2014, in Singh H. P., Prugniel P., Vauglin I., eds, ASI Conference Series, Vol. 11, International Workshop on Stellar Spectral Libraries. p. 7
Burgasser A. J., Burrows A., Kirkpatrick J. D., 2006, ApJ, 639, 1095
Cameron A. G. W., 1978, Moon Planets, 18, 5
Cheetham A. et al., 2018, A&A, 615, A160
Chun M. et al., 2008, Proc. SPIE, 7015, 70151V
Crepp J. R., Johnson J. A., Howard A. W., Marcy G. W., Brewer J., Fischer D. A., Wright J. T., Isaacson H., 2014, ApJ, 781, 29
Crepp J. R. et al., 2015, ApJ, 798, L43
Crepp J. R. et al., 2018, ApJ, 853, 192
Cruz K. L., Kirkpatrick J. D., Burgasser A. J., 2009, AJ, 137, 3345
Curtis J. L., Agüeros M. A., Mamajek E. E., Wright J. T., Cummings J. D., 2019, AJ, 158, 77
Cushing M. C., Rayner J. T., Vacca W. D., 2005, ApJ, 623, 1115
De Marchi G., Paresce F., Portegies Zwart S., 2010, ApJ, 718, 105
Delorme P. et al., 2017, A&A, 608, A79
Dohlen K. et al., 2008, Proc. SPIE, 7014, 70143L
Gagné J. et al., 2015, ApJS, 219, 33
Gaia Collaboration, 2018, A&A, 616, A1
Garcia E. V. et al., 2017, ApJ, 834, 162
Geballe T. R. et al., 2002, ApJ, 564, 466
Gorlova N. I., Meyer M. R., Rieke G. H., Liebert J., 2003, ApJ, 593, 1074
Hayashi C., Nakano T., 1963, Prog. Theor. Phys., 30, 460
Hinkley S. et al., 2015, ApJ, 805, L10
Hodapp K. W. et al., 2003, PASP, 115, 1388
Houk N., Smith-Moore M., 1988, Michigan Catalogue of Two-dimensional Spectral Types for the HD Stars, Vol. 4. Department of Astronomy, University of Michigan, Ann Arbor, MI
Houk N., Swift C., 1999, Michigan catalogue of two-dimensional spectral types for the HD Stars, Vol. 5. Department of Astronomy, University of Michigan, Ann Arbor, MI
Johnson-Groh M. et al., 2017, AJ, 153, 190
Kiefer F. et al., 2019, A&A, 631, A125
Kirkpatrick J. D., 2005, ARA&A, 43, 195
Kitzmann D., 2020, Helios-r2 – A Bayesian Nested Sampling Retrieval Code
Kitzmann D., Heng K., Oreshenko M., Grimm S. L., Apai D., Bowler B. P., Burgasser A. J., Marley M. S., 2020, ApJ, 890, 174
Konopacky Q. M. et al., 2016, ApJ, 829, L4
Kumar S. S., 1963, ApJ, 137, 1126
Lenzen R. et al., 2003, in Iye M., Moorwood A. F. M., eds, Proc. SPIE Conf. Ser. Vol. 4841, Instrument Design and Performance for Optical/Infrared Ground-Based Telescopes. SPIE, Bellingham, p. 944
Line M. R., Teske J., Burningham B., Fortney J. J., Marley M. S., 2015, ApJ, 807, 183
Macintosh B., Observatory G., 2014, American Astronomical Society Meeting Abstracts #223. p. 229.02
Maire A. L. et al., 2016, A&A, 587, A56
Maire A. L. et al., 2020, preprint (arXiv:2005.10312)
Martin E. C. et al., 2017, ApJ, 838, 73
Mawet D. et al., 2015, ApJ, 811, 103
Mawet D. et al., 2017, AJ, 153, 44
Meingast S., Alves J., Fürnkranz V., 2019, A&A, 622, L13
Mesa D. et al., 2016, A&A, 593, A119
Mesa D. et al., 2018, A&A, 612, A92
Milli J. et al., 2017, A&A, 597, L2
Nakajima T., Oppenheimer B. R., Kulkarni S. R., Golimowski D. A., Matthews K., Durrance S. T., 1995, Nature, 378, 463
Nielsen E. L. et al., 2012, ApJ, 750, 53
Oreshenko M. et al., 2020, AJ, 159, 6
Pecaut M. J., Mamajek E. E., 2016, MNRAS, 461, 794
Peretti S. et al., 2019, A&A, 631, A107
Rebolo R., Zapatero Osorio M. R., Martín E. L., 1995, Nature, 377, 129
Rickman E. L., Ségransan D., Hagelberg J., Beuzit J.-L., Cheetham A., Delisle J.-B., Forveille T., Udry S., 2020, A&A, 635, A203
Röser S., Schilbach E., 2020, preprint (arXiv:2002.03610)
Saumon D., Marley M. S., 2008, ApJ, 689, 1327
Seeliger M., Neuhäuser R., Eisenbeiss T., 2011, Astron. Nachr., 332, 821

Downloaded from https://academic.oup.com/mnras/article/495/4/4279/5843294 by guest on 01 September 2023

Slesnick C. L., Hillenbrand L. A., Carpenter J. M., 2004, ApJ, 610, 1045
Soummer R., Pueyo L., Larkin J., 2012, ApJ, 755, L28
Spiegel D. S., Burrows A., Milsom J. A., 2011, ApJ, 727, 57
Spina L. et al., 2017, A&A, 601, A70
Vázquez-Semadeni E., Palau A., Ballesteros-Paredes J., Gomez J. C., Zamora-Avilés M., 2019, MNRAS, 490, 3061
Vigan A., 2016, Astrophysics Source Code Library, record ascl:1603.001
Vigan A., Langlois M., Moutou C., Dohlen K., 2008, A&A, 489, 1345
Vigan A. et al., 2016a, A&A, 587, A55
Vigan A. et al., 2016b, Proc. SPIE, 9912, 991226
Wood C. M., Boyajian T., von Braun K., Brewer J. M., Crepp J. R., Schaefer G., Adams A., White T. R., 2019, ApJ, 873, 83
Zurlo A. et al., 2016, A&A, 587, A57

APPENDIX: ATMOSPHERIC RETRIEVAL OF HD 19467 B USING THE FULL SPECTRUM

In this Appendix, we show the retrieval for HD 19467 B using the entire spectrum, i.e. without cutting it below 1.2 μm. The derived quantities and the posterior spectra are presented in Fig. A1 while the resulting posterior distributions are shown in Fig. A2.

The results suggest that without removing the problematic region below 1.2 μm, we obtain much higher surface gravities and too small calibration factors and, therefore, radii. With a value of only 0.6 R_{Jup}, the derived median radius is probably too small for a brown dwarf. While we still obtain subsolar C/O ratios, the overall metallicity is now supersolar. The posterior spectra shown in bottom panel of Fig. A1 corroborate our previous approach of removing the peak around 1 μm from our retrieval analysis. It is clear, that the model has problems fitting this spectral region.

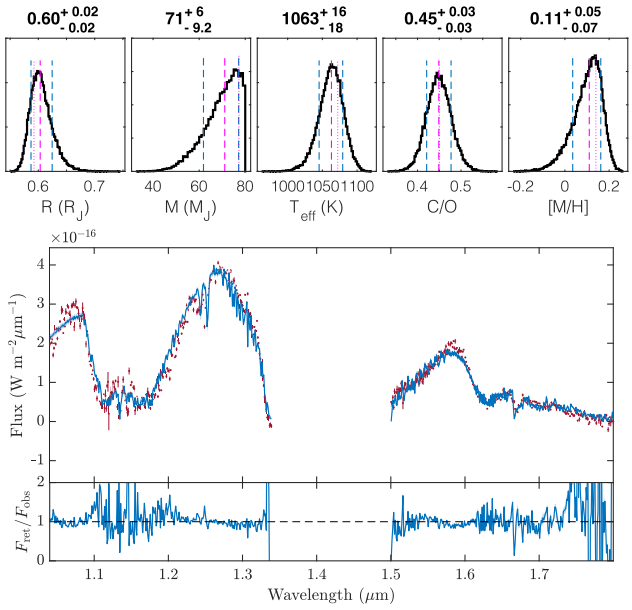

Figure A1. *Top*: Posterior distributions of derived quantities for the retrieval of HD 19467 B. The posteriors are shown for the brown dwarf radius R, its mass M, effective temperature T_{eff}, the C/O ratio, and the overall metallicity [M/H]. *Bottom*: Posterior spectra and residuals. The solid lines refer to the median of all posterior spectra. The shaded areas signify the 3σ confidence intervals of the spectra. The measured spectrum is indicated by the red data points.

Downloaded from https://academic.oup.com/mnras/article/495/4/4279/5843294 by guest on 01 September 2023

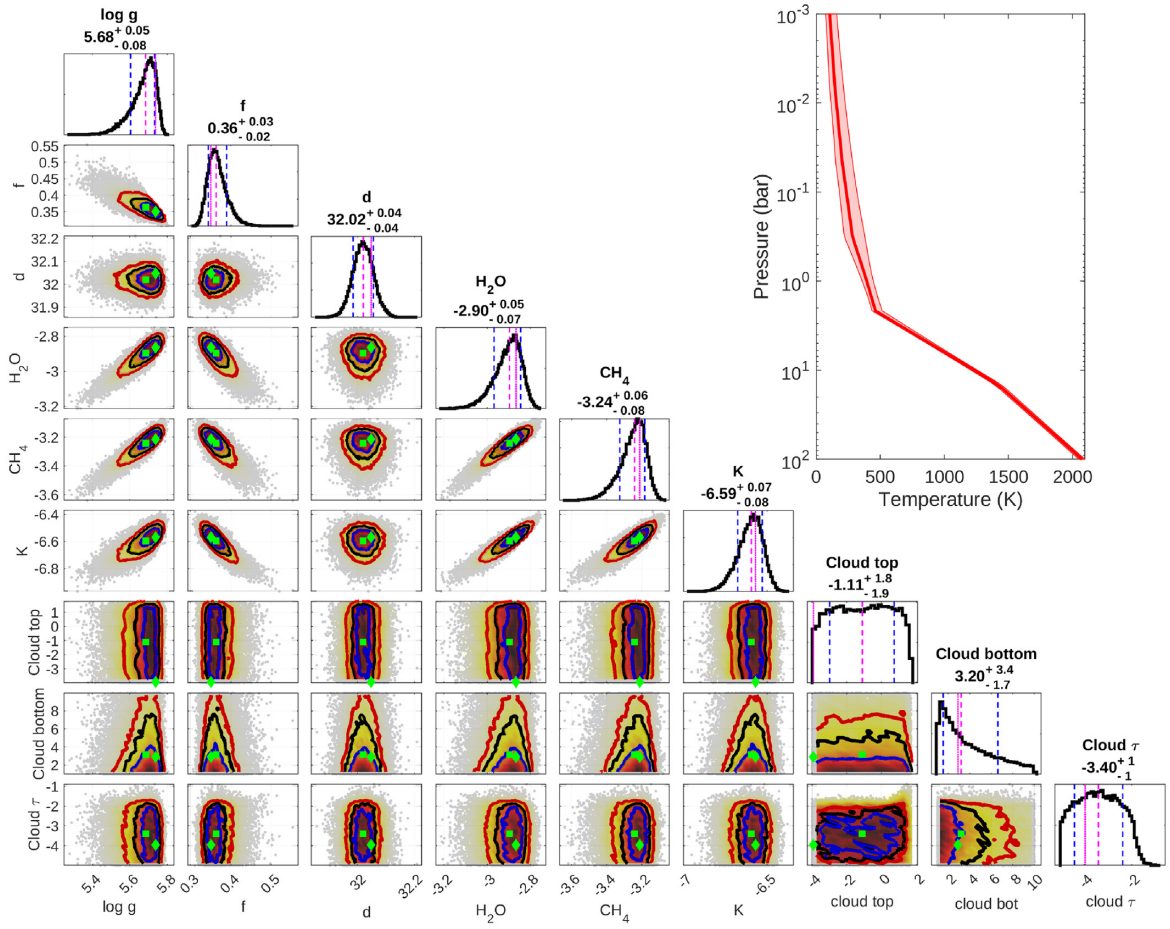

Figure A2. Posterior distributions for the retrieval of HD 19467 B using the full available spectrum. See caption of Fig. 11 for details on the posterior plots.

This paper has been typeset from a TEX/LATEX file prepared by the author.

Downloaded from https://academic.oup.com/mnras/article/495/4/4279/5843294 by guest on 01 September 2023